Parameterization of Tropical Cirrus Ice Crystal Size Distributions and Implications for Radiative Transfer: Results from CEPEX

GREG M. MCFARQUHAR AND ANDREW J. HEYMSFIELD

National Center for Atmospheric Research, Boulder, Colorado*

(Manuscript received 2 August 1996, in final form 23 December 1996)

ABSTRACT

Average ice crystal size distributions are parameterized as functions of temperature and ice water content (IWC), based on observations in cirrus produced as outflows of deep convection made during the Central Equatorial Pacific Experiment (CEPEX), as the sum of a first-order gamma function, describing ice crystals with melted equivalent diameters (D_m) less than 100 μm, and a lognormal function, describing larger ice crystals. The fit parameters are chosen to minimize the chi-squared function describing the difference between observed and parameterized distribution functions. The parameterization is mass conserving, accurately represents small ice crystals, and is easily integrable.

The parameterization gives accurate estimates of mass, area, and number contained in different size ranges. The radiative properties estimated from midlatitude parameterizations are compared with those estimated from this parameterization using anomalous diffraction theory. As opposed to some previous studies, small crystals do not dominate the mass and radiative properties of cirrus. Comparison with midlatitude observations shows that size distribution shape can vary substantially depending on where, when, and how the cirrus is measured and on how it forms.

1. Introduction

The Committee on Earth Science of the U.S. Global Change Research Program (Committee on Earth Sciences 1989) has identified the role of clouds as the highest priority item needing improvement in the study of the earth's climate system. Ice clouds, especially tropical cirrus, have been shown in general circulation model (GCM) and satellite studies to have a major effect on the earth's radiation balance and climate as the result of the significant contribution they make to diabatic heating in the upper troposphere (Ramaswamy and Ramanathan 1989). The radiative properties of ice clouds are influenced to a large extent by the cloud microphysics (Stephens et al. 1990), which, in the Tropics, is influenced by convection that produces much of the cirrus. However, realistic parameterizations of cirrus microphysical and radiative properties and their relation to the convection producing them are largely unavailable.

Data upon which parameterizations can be based have been lacking since tropical cirrus are usually inaccessible because they are far removed from aircraft landing sites and because they extend to very high altitudes. Recent measurements made during the Central Equatorial Pacific Experiment (CEPEX), reported by Heymsfield and McFarquhar (1996), hereafter HM, and McFarquhar and Heymsfield (1996), hereafter MH, considerably expand the data available by giving information on the numbers, sizes, and shapes of ice crystals both larger (measured by optical array probes) and smaller (measured by the Video Ice Particle Sampler, VIPS) than 100 μm in tropical cirrus, some of which were remnants from deep convection. Other measurements of ice crystal distributions include those made by Knollenberg et al. (1982), Knollenberg et al. (1993), Heymsfield (1986), and Griffith et al. (1980), but all of these measurements are made over a more narrow range of temperatures.

This study is similar to that reported by Heymsfield and Platt (1984), hereafter HP, who used a cirrus cloud dataset to show that both the form of the size distributions and crystal habits changed systematically with temperature. Their study relied primarily on data collected in midlatitude cirrus formed in situ (Heymsfield 1977), and the size distribution parameterization was developed only for crystal dimensions greater than 20 μm. These crystal size distributions were used by Platt and Harshvardhan (1988) in their parameterization of cirrus cloud radiative properties, where the properties are only a function of temperature, and by Ebert and

* The National Center for Atmospheric Research (NCAR) is sponsored by the National Science Foundation.

Corresponding author address: Dr. Greg M. McFarquhar, NCAR/MMM, P.O. Box 3000, Boulder, CO 80307-3000
E-mail: mcfarq@ncar.ucar.edu

Curry (1992), hereafter EC, in their parameterization of ice cloud optical properties, which allows the ice water path (IWP) and effective radius (r_e) to be varied independently. There have been no similar studies as of yet using ice crystal size distributions measured in the Tropics, nor for cirrus formed as the result of deep convection.

Parameterization of crystal size distributions, and the accompanying information about the ice crystals' radiative properties, in terms of ice water content (IWC) and temperature are useful because many GCMs now use IWC as a prognostic variable (e.g., Sundqvist 1978; Roeckner et al. 1987). Hence, parameterizations in terms of IWC can be used to obtain other information diagnostically. Detailed parameterizations of ice crystal size distributions are also required for microphysical models with explicit microphysics. Very precise radiative calculations of the effects of ice crystals on solar (Liou and Takano 1994) and infrared (Chylek and Videen 1994) radiation also require a detailed knowledge of the sizes and shapes of ice crystals.

2. Ice crystal measurements from CEPEX

a. How measurements were obtained

In situ measurements of cirrus anvils were an essential component of CEPEX. The Aeromet Learjet, which was equipped with a complement of instruments to measure the microphysical and radiative properties of clouds, flew 35 h in cloud, approximately one-third of which was spent near cloud tops. The measurements were taken within the area bounded by 20°S–2°N and 165°E–170°W. The ambient temperatures ranged between −70°C and −20°C.

Heymsfield and McFarquhar (1996) and MH describe the measurements and the instruments used to acquire the data in more detail. In this study, data from the Particle Measuring System's two-dimensional cloud probe (2DC) and from the VIPS are used. One bin width (40 μm) is added to the length of each 2DC particle to account for the probe start-up time. Hobbs et al. (1996) discuss the severe limitations of the 2DC for measuring ice crystals smaller than 100 μm in dimension, especially for the high airspeeds (approximately 200 m s^{-1}) at which the Learjet flew. Hence, only crystals larger than 100 μm dimension measured by the 2DC are considered in this study.

Information about small particles with dimensions between 5 and 150 μm is obtained from the VIPS, a probe designed to measure small ice crystals. Images of crystals that impact on a transparent moving belt exposed to the airflow are recorded by two videomicroscopes, digitized, and later analyzed using research grade imaging software designed by the National Institute of Health. Crystals larger than about 150 μm tend to break upon impact, making it difficult to determine their original shape; their low concentrations also make it difficult to obtain a sufficiently large statistical sample. The availability of analyzed data from the VIPS is limited because data reduction is not automated; each crystal must be individually sized and measured.

b. Derived parameters from measurements

McFarquhar and Heymsfield (1996) describe the microphysical parameters that can be derived from the 2DC and VIPS measurements. A number of different measures can be used to represent an ice crystal measured by a probe, including a maximum crystal dimension ($D_{\max}$), an area ratio (ar), and an area-equivalent diameter (D_a). The parameterization introduced here is based primarily upon distributions of mass-equivalent spheres, with diameter, D_m, given by

$$D_m = \sqrt[3]{\frac{6M}{\pi\rho_{\text{ice}}}}, \tag{1}$$

where M is the mass of the ice crystal determined from the maximum crystal length and area ratio using habit-dependent mass diameter relationships, and ρ_{ice} is the density of solid ice spheres, assumed to be 0.91 g cm^{-3}.

For a population of ice crystals, MH and HM also defined effective diameter (D_e), IWC, volume extinction coefficient (β_{ext}), and cross-sectional area (A_c). The contributions of particles to radiative properties, such as the volume extinction coefficient, are closely related to the projected areas those particles present to incoming radiation. Because this parameterization is principally based upon distributions of mass-equivalent spheres, it is convenient to also define the cross-sectional area from the distribution of equivalent melted spheres, A_s, as

$$A_s = \frac{\pi}{4}\int_0^\infty N(D_m)D_m^2\, dD_m, \tag{2}$$

where $N(D_m)$ represents the number distribution function for particles with mass-equivalent diameter D_m.

In this paper, radiative properties, such as β_{ext}, volume absorption coefficient (β_{abs}), single scatter albedo ($\tilde{\omega}_0$), and infrared emissivity (ϵ), are calculated using anomalous diffraction theory (ADT) developed by van de Hulst (1956), following the equations outlined by Mitchell and Arnott (1994). Tables giving the complex index of refraction as a function of wavelength are found in Warren (1984). Following EC, the shortwave spectrum is divided into five spectral intervals for calculations: 0.25–0.7, 0.7–1.3, 1.3–1.9, 1.9–2.5, and 2.5–3.5 μm. The fractions of solar irradiance at the top of the atmosphere in each spectral band are given by Thekaekara and Drummond (1971).

3. Parameterization techniques

a. Need for parameterization

The goal of the parameterization is to characterize the radiative effects of tropical ice crystal size distri-

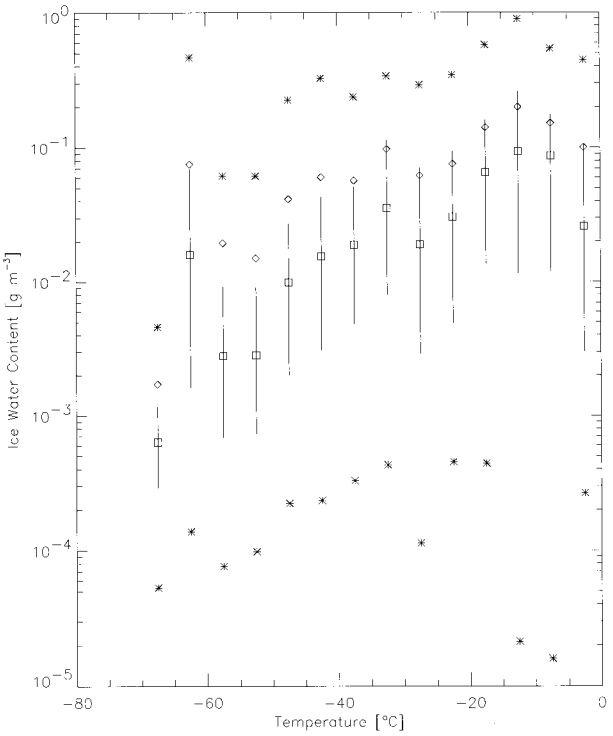

FIG. 1. Average IWC (diamonds) for 5°C wide bins, deduced from 10-s averages of all CEPEX observations. Solid lines run between first and third quartile of IWC distribution, squares represent medians, and asterisks represent outliers (5 and 95 percentiles of distribution).

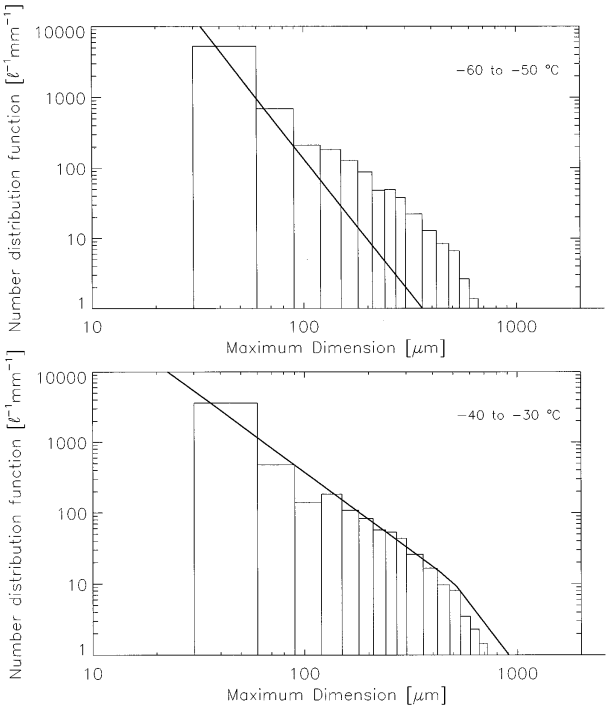

FIG. 2. Average number distribution function against maximum crystal dimension for the average ice crystal size distribution measured during CEPEX with IWCs between $10^{-1.5}$ and 10^{-1} g m^{-3} for temperatures between (a) −60° and −50 °C, and (b) −40° and −30°C. Heymsfield and Platt (1984) parameterization superimposed with solid line.

butions given the ice water content IWC and temperature *T*. Figure 1 demonstrates why size distributions from these clouds cannot be parameterized as functions of *T* alone; average IWCs for 5°C wide bins as a function of *T* are displayed based on CEPEX data. Each point contributing to the data set is a 10-s average (or 2-km horizontal distance) of all particles detected by the 2DC during that period. Time periods where significant numbers of spurious images were recorded by the 2DC have been removed. Heymsfield and McFarquhar (1996) describe the different cloud conditions in which the measurements were made. IWC varies widely within each bin; the quartiles for the IWC distribution within each bin typically differ from the means by more than one order of magnitude, and the range between the outliers (5 and 95 percentiles) is frequently three to four orders of magnitude. This is expected because measurements were taken in cumulus-anvil complexes with varying intensities, at varying growth stages, and at varying distances below cloud top; some measurements taken in cirrus whose origin was not identified are also included in the averages. Average IWCs are typically an order of magnitude greater than median IWCs, indicating that average IWC is dominated by the contributions of a few large IWC cases; hence, the representativeness of average IWC for characterizing clouds may be questioned. In any event, the wide variation of IWC within a single *T* bin shows that it is difficult to characterize size distributions as a function of *T* alone. Therefore, size distributions are characterized as functions of *T* and IWC.

Heymsfield and Platt (1984) introduced a preliminary scheme for parameterizing cirrus particle size distributions for crystal dimensions greater than 20 μm as a function of temperature using data reported by Heymsfield (1977). They noted that the form of the size distributions changed systematically with temperature. Figure 2 shows average size distributions, measured by the 2DC during CEPEX, with IWCs between $10^{-1.5}$ and $10^{-1.0}$ g m^{-3}, for the indicated temperature ranges, compared to size distributions calculated from HP's parameterization. The better agreement between measurements and parameterizations at temperatures greater than −40°C compared to temperatures less than −40°C is observed for several IWC ranges. Differences are expected at the lower temperatures because different physical processes are involved in cirrus formation; tropical cirrus frequently originate as the outflow of deep convective cores, whereas midlatitude cirrus are principally produced by in situ lifting and localized convection. In addition, the tropopause extends to much higher altitudes in the Tropics. McFarquhar and Heymsfield (1996) noted substantial horizontal inhomogeneities in clouds observed during CEPEX on scales less than 100 km, whereas HP noted that much of their data came from horizontally uniform clouds. The changes

that occur in the shape of the size distribution as temperature varies are much less substantial for the CEPEX data compared to the HP parameterization. Hence, it was apparent that a new parameterization for ice crystal size distributions in the Tropics was needed to characterize the CEPEX measurements.

b. Previous parameterizations

Many functions have been used to describe the size distribution of ice crystals and droplets in stratiform and cirrus clouds. Dowling and Radke (1990) obtained a formula for typical particle size distributions by fitting a curve by eye and adjusting it so that the number- and mass-weighted crystal dimensions were consistent with typical observations. Gamma and exponential functions have also been used to describe observed distributions of cloud particles. Borovikov et al. (1963) utilized gamma distributions to describe droplet size distributions in stratiform and stratocumulus clouds. Many useful parameters, such as concentration, liquid water content, and modal radius, can be derived from the gamma distribution parameters. The case $n = 2$ represents a special case called the Khrgian–Mazin distribution and is commonly used to describe the distribution function for small cloud droplets. Kosarev and Mazin (1989) used gamma distributions with orders between 0 and 2 to describe the cirrus cloud particle size distributions that they observed. Welch et al. (1980) and others have also parameterized ice crystal size distributions as modified gamma distributions.

c. Parameterization concept

In order for the parameterization of tropical ice crystal size distributions to have the maximum utility and accuracy for modeling and climate studies, four major requirements were identified: first, the optical and radiative properties from the parameterized size distributions had to replicate those from the observed size distributions as closely as possible; second, mass conservation was required (i.e., the mass of the parameterized size distribution had to be the same as the mass of the observed size distributions); third, the contributions of the smaller ice crystals had to be realistically represented; and fourth, the parameterization had to be easily integratable over all possible crystal sizes (i.e., from 0 to infinitely large crystals) and converge, so that it could be easily implemented in numerical models. The latter point is especially important since, for example, HP's parameterization gives an adequate representation of the size distributions down to 20 μm, but extending their fits to 0 μm gives unreasonably large total numbers and masses.

The parameterization introduced here depends on mass-equivalent dimension rather than on maximum crystal length to more easily force mass conservation. The fit parameters were constrained so that the mass of any parameterized size distribution was equal to the mass contained in the original size distribution. However, the radiative properties obtained from this parameterization do not assume equivalent melted spheres or equivalent area spheres.

The distributions of large and small ice crystals are represented separately. ''Large'' ice crystals, with $D_m > 100$ μm, were measured by the 2DC, and ''small'' ice crystals, with $D_m < 100$ μm, were measured by the VIPS. Particles with $D_m < 100$ μm measured by the 2DC and with $D_m > 100$ μm measured by the VIPS were not used in the analysis.

All 2DC spectra, each representing a 10-s or 2-km average, were grouped into 6 temperature bins, spaced every 10°C starting at −70°C, and into 10 logarithmically spaced IWC bins (10^{-6} to 10^{-4}, 10^{j} to $10^{j+0.5}$ g m^{-3}, where $j = i/2 - 4$, $i = 0, \cdots, 9$). Averaging in different IWC ranges allows a determination if shape conservation of size distribution with IWC exists. The temperatures at which the measurements were made are not necessarily the temperatures at which the ice crystals grew because they may have been lifted to those levels by convection or may have fallen to those levels from higher heights.

There were not sufficient data to group and average the small crystal size distributions measured by the VIPS into different IWC and T bins; only 37 size distributions, each representing a 6-s average, have been processed at this time. Instead, each size distribution was fit independently, and then the variation of the fit parameters as a function of IWC was examined; the analyzed VIPS measurements do not exist over a wide enough temperature range to look for trends with T.

Because there were minimal VIPS data, the locations and times at which data were obtained are examined to determine their representativeness. The data were obtained on 1, 4, and 5 April from the upper regions of anvils. Figure 3 shows the cloud boundaries of the upper layers for times at which VIPS measurements were made on 4 April. Only the upper parts of the clouds are shown because the data were obtained with a Nd:YAG lidar (Spinhirne and Hart 1990), which is occulted by optical depths greater than about three (Kinne et al. 1992). The measurements acquired on 4 April were mostly from parts of runs about 2 km below cloud top; the displacement above cloud bottom cannot be determined because the lidar beam is attenuated. The 1 and 5 April data were acquired in thinner clouds with lower IWCs and near cloud tops as reported by the flight scientists (A. Buckholtz and D. Rusk personal communication, 1993). This suggests that the data were acquired over a variety of conditions found near the tops of anvils. There are no data from warmer temperatures and from lower regions of the anvils because the VIPS becomes saturated from the abundance of crystals under such high IWC conditions, meaning that individual images could not be distinguished. Heymsfield and McFarquhar (1996) show that larger crystals tend to

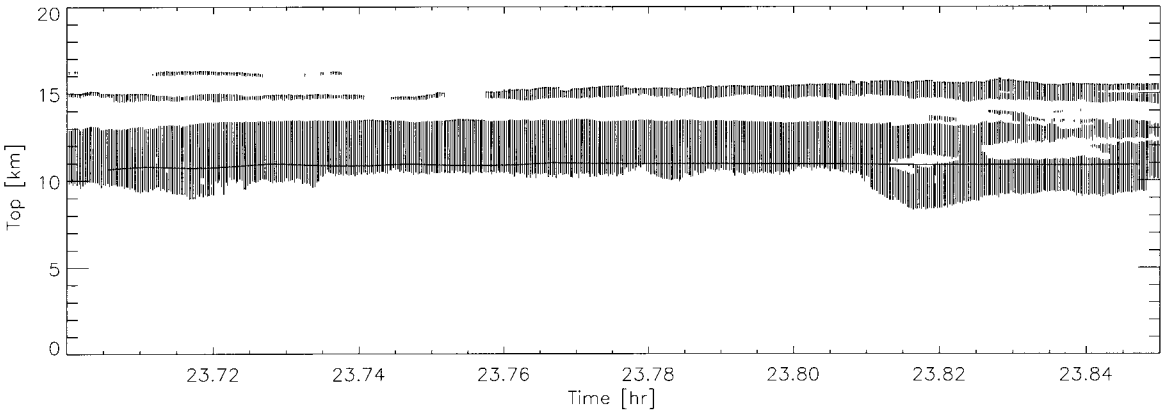

FIG. 3. Cloud layers detected by 0.532-μm Nd:YAG lidar (courtesy of J. D. Spinhirne and W. D. Hart), with flight path of Learjet superimposed (solid line). Data acquired 4 April during CEPEX.

dominate under such conditions; hence, the absence of small crystal measurements is not a major caveat as they do not contribute substantially to the radiative properties.

Tests determined that first-order gamma distributions best characterized small crystals and lognormals well represented large crystals. However, it should be emphasized that two functions cannot completely describe all possible ice crystal size distributions; this parameterization only describes the functions that best fit the average properties of the observed size distributions. The first-order gamma function characterizing the small ice crystals measured by the VIPS is given by

$$N(D_m) = \frac{6\mathrm{IWC}_{<100}\alpha_{<100}^5 D_m}{\pi\rho_{\mathrm{ice}}\Gamma(5)}\exp(-\alpha_{<100}D_m), \quad (3)$$

where $\alpha_{<100}$ is a parameter of the first-order gamma distribution and $\mathrm{IWC}_{<100}$ is the mass of all crystals smaller than 100 μm in the observed size distribution. Equation (5), introduced later, gives $\mathrm{IWC}_{<100}$ as a function of total IWC, IWC_T. Equation (3) is written in the above form so that the integral of the mass over all crystal sizes ($0 \rightarrow \infty$) is equal to $\mathrm{IWC}_{<100}$. The function can be applied over the complete range of sizes (even though it is only designed to represent small crystals) because the numbers of large crystals given by this distribution are very small, as will be shown later. The subscript <100 emphasizes that this exponential is designed only to describe the contributions of crystals smaller than 100 μm. The lognormal function is given by

$$N(D_m) = \frac{6\mathrm{IWC}_{>100}}{\pi^{3/2}\rho_{\mathrm{ice}}\sqrt{2}\exp(3\mu_{>100} + (9/2)\sigma_{>100}^2)D_m\sigma_{>100}D_0^3} \times \exp\left[-\frac{1}{2}\left(\frac{\log\frac{D_m}{D_0} - \mu_{>100}}{\sigma_{>100}}\right)^2\right], \quad (4)$$

where $\mathrm{IWC}_{>100}$ is the mass of all crystals with D_m greater than 100 μm in the observed size distributions, $D_0 = 1$ μm a parameter used to ensure that the equation does not depend on the choice of units for D_m, $\sigma_{>100}$ the geometric standard deviation of the distribution, and $\mu_{>100}$ the location of the mode. Both $\sigma_{>100}$ and $\mu_{>100}$ depend on the choice of $D_0 = 1$ μm. The lognormal function, although designed to represent crystals larger than 100 μm, is also applied over the complete range of sizes because the number distribution function for smaller sizes is minimal for the choice of parameters that match the CEPEX data.

The appendix describes the fitting techniques that were used to determine the fit parameters as a function of temperature and IWC_T. They involved the minimization of the chi-squared function with uncertainties determined from the bootstrap method (Efron and Tibshirani 1993), a modified Monte Carlo technique.

4. Parameterization results

The relative weightings of the lognormal and gamma distributions are determined from the respective IWCs of the large and small crystals. Figure 4 plots $\mathrm{IWC}_{<100}$ as a function of total $\mathrm{IWC}_T = \mathrm{IWC}_{<100} + \mathrm{IWC}_{>100}$, where the 100-$\mu m$ threshold is for D_m. The solid line represents the least-squares fit to the data. $\mathrm{IWC}_{<100}$ can be estimated from IWC_T using

$$\mathrm{IWC}_{<100} = \min\left[\mathrm{IWC}_T, a\left(\frac{\mathrm{IWC}_T}{\mathrm{IWC}_0}\right)^b\right], \quad (5)$$

where $a = 0.252 \pm 0.068$ g m^{-3}, $b = 0.837 \pm 0.054$, and $\mathrm{IWC}_0 = 1$ g m^{-3}. The uncertainty estimates were calculated assuming all points are weighted equally and assuming that a good fit to the data existed. As expected, smaller crystals make larger contributions to the total mass for lower IWC_T. It is necessary to ensure that $\mathrm{IWC}_{<100}$ is not greater than IWC_T. Although $\mathrm{IWC}_{<100}$ in Eq. (5) may also be a function of T, there were not sufficient data to characterize such a relationship.

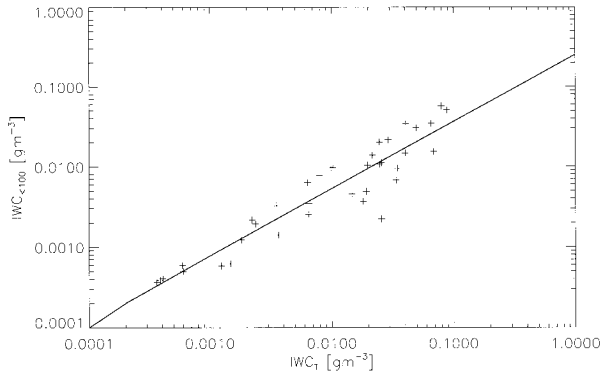

FIG. 4. IWC$_{<100}$ vs total IWC$_T$ = IWC$_{<100}$ + IWC$_{>100}$. Solid line represents best fit to data.

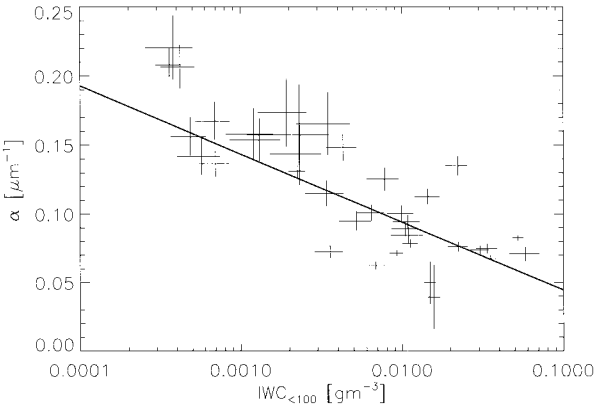

FIG. 6. Slope of exponential distribution obtained from fits to VIPS data as function of IWC$_{<100}$. Bars on each point represent error bars. Solid line represents best fit to α − IWC$_{<100}$ data.

Figure 5 shows an example of the best exponential fit to a small crystal spectrum measured using the VIPS in a thin anvil cloud. As mentioned previously, no size distributions were available for conditions of large IWC$_T$ or IWC$_{<100}$. Figure 6 shows how $\alpha_{<100}$ varies with IWC$_{<100}$. The error bars in the data points are the standard deviations of $\alpha_{<100}$ and IWC$_{<100}$ obtained from the bootstrap technique. Note that $\alpha_{<100}$ becomes smaller as IWC$_{<100}$ increases. The large variability seen is expected as the numbers and masses of small crystals vary a lot in nature (Arnott et al. 1994; MH). The solid line indicates the best fit to the data obtained by considering the errors in both coordinates (Press et al. 1992, 660):

$$\alpha_{<100} = b - m \log_{10}\left(\frac{\text{IWC}_{<100}}{\text{IWC}_0}\right), \qquad (6)$$

where $b = -4.99 \times 10^{-3} \pm 5.50 \times 10^{-3}$ μm^{-1} and $m = 0.0494 \pm .0029$ μm^{-1}. The χ^2 for the fit is 433 with 37 degrees of freedom, suggesting that a unique relationship of this form is not justified by the data. This indicates that the natural variability of the size distributions can extend beyond the uncertainties of the fit and that therefore the parameterization only represents significant dependences in the data on an average basis.

When the average size distributions obtained from the 2DC were fit to lognormal distributions for each IWC and T bin, the observed number distribution functions for sizes with D_m less than 100 μm were set to zero because small crystals are already accounted for in the VIPS parameterization and because small crystals are not accurately measured by the 2DC. The initial guesses for the mode and breadth of the lognormal distributions that are required for the simplex fitting procedure were estimated following the approach described by Feingold and Levin (1986).

Figure 7 shows the average size distribution for T between −50° and −40°C and for IWC$_{>100}$ between 10^{-1} and $10^{-0.5}$ g m^{-3}, together with the best fit. No explicit comparison can be made with the HP parameterization because their number distribution functions are not expressed in terms of D_m.

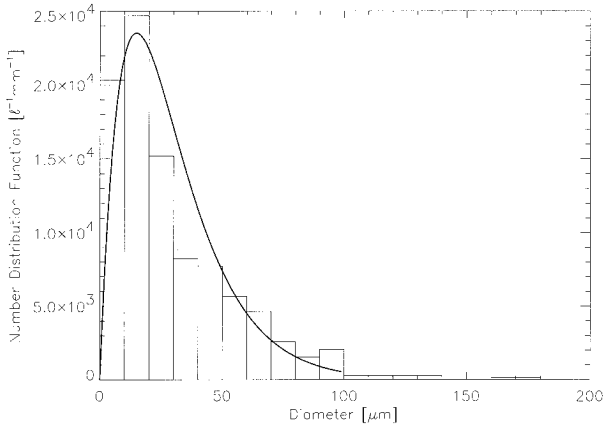

FIG. 5. Ice crystal spectrum calculated from VIPS measurements 1 April 2304:54 to 2305:00 UTC. Horizontal axis is melted equivalent diameter. Temperature −43.9°C. Solid line represents best fit to data conserving mass. Only crystals with $D_m < 100$ μm used in fit.

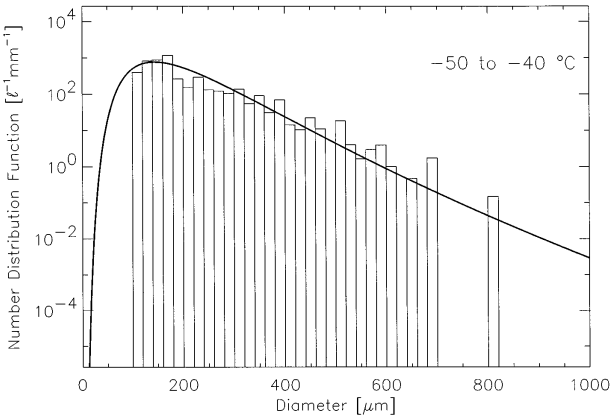

FIG. 7. Average ice crystal size distribution observed during CEPEX with IWC between 10^{-1} and $10^{-0.5}$ g m^{-3} and T between −50 and −40°C. Horizontal axis melted equivalent diameter. Solid line represents best fit of mass conserving lognormal distribution. Points with $D_m < 100$ μm do not contribute to the fit.

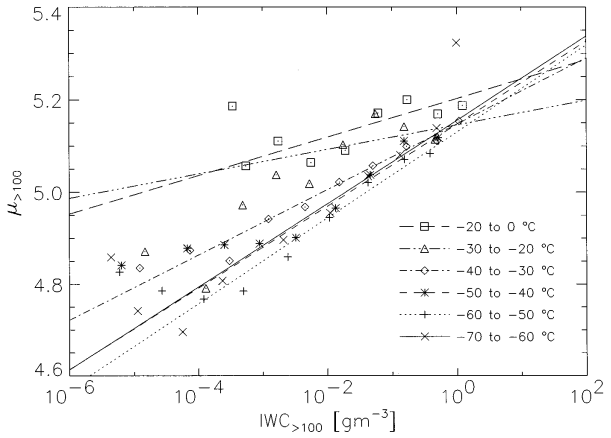

FIG. 8. Mode of lognormal distribution $\mu_{>100}$ as function of IWC, with different symbols representing temperatures at which measurements made. Different type lines represent best fit to data for each temperature.

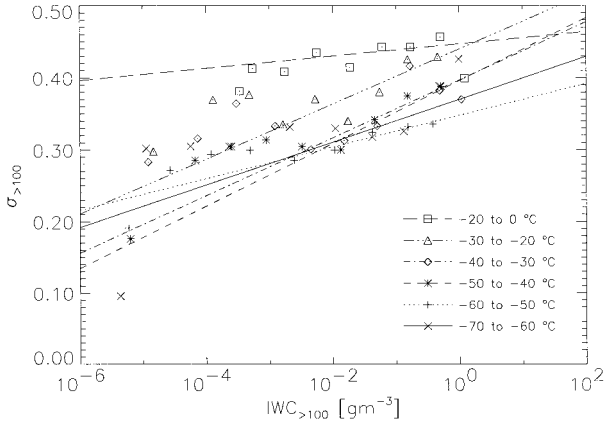

FIG. 9. As in Fig. 8 except for breadth of lognormal distribution, $\sigma_{>100}$.

Figure 8 shows the variation of the mode of the lognormal distribution $\mu_{>100}$ with $IWC_{>100}$ and temperature. The symbols represent the data points, and the different line types represent the best fit to the data at each temperature; the fit coefficients are given in Table 1. For a given temperature, $\mu_{>100}$ is given by

$$\mu_{>100} = a_\mu(T) + b_\mu(T)\log_{10}\left(\frac{\mathrm{IWC}_{>100}}{\mathrm{IWC}_0}\right), \qquad (7)$$

where $a_\mu(T)$ and $b_\mu(T)$ are temperature dependent. The error bars in both directions on the data points were considered in the calculations of the fits but are not explicitly shown so that measurements at different temperatures can be distinguished. The error bars were typically very small, particularly for those points where many size distributions (greater than 50) were used to calculate the averages. The high values of χ^2 (Table 1) indicate that the fits do not account for all variability in the data; however, the fits represent significant dependencies in the data.

Trends in Fig. 8 are clear. The mode shifts to larger values for larger IWCs and higher temperatures. This is consistent with HM's analysis showing larger crystals at higher IWCs and higher temperatures.

Figure 9 illustrates how the breadth of the lognormal distribution varies with IWC and temperature; the coefficients of the temperature-dependent fits are given in Table 2. For a given temperature, $\sigma_{>100}$ is expressed as

$$\sigma_{>100} = a_\sigma(T) + b_\sigma(T)\log_{10}\left(\frac{\mathrm{IWC}_{>100}}{\mathrm{IWC}_0}\right), \qquad (8)$$

where $a_\sigma(T)$ and $b_\sigma(T)$ are obtained from the fits minimizing χ^2. The relative uncertainties in $\sigma_{>100}$ are similar to those in $\mu_{>100}$. It is seen that $\sigma_{>100}$ increases as temperature and IWC increase. It is to be expected that the size distributions are broader when more large crystals are present.

In order to provide the parameterization in a form convenient for incorporation into models, the coefficients of the fits used in Eqs. (7) and (8) must be further expressed as a function of temperature. To parameterize a_μ, b_μ, a_σ, and b_σ as functions of temperature, linear fits as a function of temperature minimizing χ^2 are performed. Because the calculated errors in a_μ, b_μ, a_σ, and b_σ do not realistically represent the spread in the data, the weighting for a_μ, b_μ, a_σ, and b_σ at each temperature was proportional to the number of measurements made at each temperature rather than using the calculated errors. Figure 10 shows a_μ, b_μ, a_σ, and b_σ as functions of temperature, and the best fits to the data, given by

TABLE 1. Fit coefficients for Eq. (7) obtained from least squares fits.

Temperature (°C)	a_μ	δa_μ	b_μ	δb_μ	χ^2
−70 to −60	5.156	.007	.091	.005	48.
−60 to −50	5.131	.004	.093	.002	254.
−50 to −40	5.148	.006	.089	.003	95.
−40 to −30	5.148	.005	.071	.003	11.
−30 to −20	5.146	.006	.027	.005	94.
−20 to 0	5.203	.005	.042	.004	85.

TABLE 2. Fit coefficients for Eq. (8) obtained from least-squares fits.

Temperature (°C)	a	δa	b	δb	χ^2
−70 to −60	.370	.004	.030	.002	149.
−60 to −50	.348	.003	.022	.001	45.
−50 to −40	.396	.004	.044	.002	98.
−40 to −30	.397	.004	.040	.003	169.
−30 to −20	.440	.007	.038	.005	20.
−20 to 0	.447	.003	.008	.003	65.

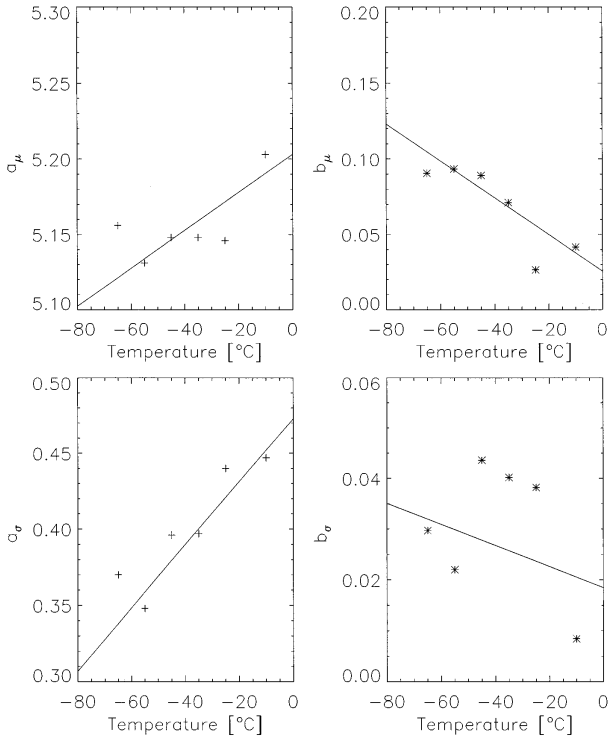

FIG. 10. Variation of a_μ, b_μ, a_σ, and b_σ with temperature shown with linear fits to data minimizing χ^2. Weights for fits proportional to number of measurements at each temperature.

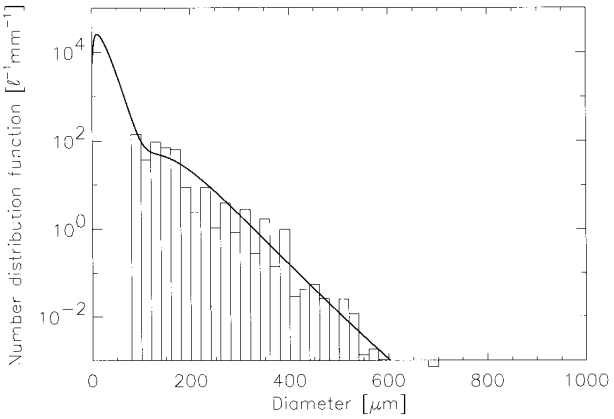

FIG. 11. Average crystal size distribution observed by 2DC with $-40°C < T < -50°C$ and $10^{-2} < \text{IWC} < 10^{-1.5}$, with parameterized size distribution for $T = -45°C$ and $\text{IWC}_T = 0.024$ g m^{-3}; representative VIPS size distribution not known for such conditions.

$$a_\mu(T) = a_{a_\mu} + b_{a_\mu}T, \tag{9}$$

$$b_\mu(T) = a_{b_\mu} + b_{b_\mu}T, \tag{10}$$

$$a_\sigma(T) = a_{a_\sigma} + b_{a_\sigma}T, \tag{11}$$

$$b_\sigma(T) = a_{b_\sigma} + b_{b_\sigma}T, \tag{12}$$

with the coefficients of the fit given by $a_{a_\mu} = 5.20 \pm .02$, $b_{a_\mu} = 0.0013 \pm .0005$, $a_{b_\mu} = 0.026 \pm .023$, $b_{b_\mu} = -1.2 \pm 0.5 \times 10^{-3}$, $a_{a_\sigma} = 0.47 \pm .02$, $b_{a_\sigma} = 2.1 \pm .5 \times 10^{-3}$, $a_{b_\sigma} = 0.018 \pm .023$, and $b_{b_\sigma} = -2.1 \pm 4.7 \times 10^{-4}$. The units of the a terms are the natural logarithm of μm; for the b terms, the natural logarithm of μm °C^{-1}. For some of these coefficients, the uncertainties are equal to the parameter values, indicating that they have minimal variation with temperature. However, the smaller uncertainties in a_{a_μ} and a_{a_σ} show definite variations with temperature, reflecting the dependence of $a_\mu(T)$ and $a_\sigma(T)$ with temperature in Figs. 8 and 9.

Hence, given any T and IWC, the size distribution can be determined using the sum of the gamma and lognormal distributions. The summed distribution can be easily integrated over the complete range of crystal sizes to describe total mass or area. Figure 11 shows an example for $T = -45°C$ and $\text{IWC}_T = 0.024$ g m^{-3} of the average size distribution measured by the 2DC with temperature between $-40°C$ and $-50°C$ and with IWC_{2DC} between 10^{-2} and $10^{-1.5}$ g m^{-3} (average IWC_{2DC} for $D_m > 100$ μm is 0.013 g m^{-3}, corresponding to IWC_T of 0.024 g m^{-3} above). Even though the average observed VIPS size distribution with $D_m < 100$ μm cannot be ascertained for this case, it was previously seen that the small crystal population is well represented by the parameterization for the small IWCs where the VIPS measurements were obtained.

For the calculation of radiative properties (e.g., volume extinction and absorption characteristics), the actual cross-sectional area rather than the area of equivalent melted spheres must be known. Hence, A_c and A_s calculated from the observed size distributions were compared. For small crystals with $D_m < 100$ μm measured by the VIPS and represented by an exponential function, there was only a 4% difference between A_c and A_s on average. There was no noticeable trend for how the ratio A_c/A_s varied with $\text{IWC}_{<100}$. Hence, no adjustments to the parameterized radiative properties were needed.

However, differences between A_c and A_s for crystals with $D_m > 100$ μm measured by the 2DC were more substantial. Figure 12 shows A_c/A_s against $\text{IWC}_{>100}$ for different temperature ranges, with best fits to the data, given by

$$A_c/A_s = \max\left[1.0,\ a(T) + b(T)\log_{10}\left(\frac{\text{IWC}_{>100}}{\text{IWC}_0}\right)\right], \tag{13}$$

where $a(T)$ and $b(T)$ are the temperature-dependent coefficients of the fit given by

$$a(T) = a_{a_T} + b_{a_T}T, \tag{14}$$

$$b(T) = a_{b_T} + b_{b_T}T, \tag{15}$$

with $a_{a_T} = 2.539 \pm .030$, $b_{a_T} = 0.0177 \pm .0007$ °C^{-1}, $a_{b_T} = 0.285 \pm .024$, and $b_{b_T} = 1.3 \pm 0.5 \times 10^{-4}$ °C^{-1}. The ratio A_c over A_s is forced to be greater than or equal to 1.0 because ratios less than 1.0 are not physically realistic. The χ^2 for the fits are larger than the number

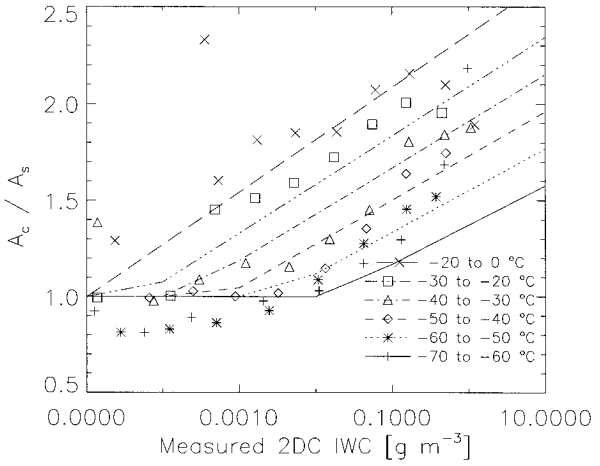

FIG. 12. Ratio A_c/A_s from each of 57 observed size distributions as function of IWC; different symbols represent different temperatures. Lines represent best fits from Eqs. (13) through (15).

of degrees of freedom, showing again that the fits only represent significant dependencies in the data and do not account for all of the variability. The error bars in A_c, A_s, and $\mathrm{IWC}_{>100}$ considered in the least-squares minimization of fit parameters were again determined from the bootstrap approximation, and the weightings of the temperature-dependent fit parameters used in the determination of a_{a_T}, b_{a_T}, a_{b_T}, and b_{b_T} in Eqs. (14) and (15) were given by the number of measurements at each temperature. The fits replicate the data reasonably well, especially at large IWCs where the radiative effects are most important; in general, the A_c/A_s ratio is larger for greater IWCs because there are more larger crystals, which tend to be aspherical. At warmer temperatures there are more rimed crystals which are also more aspherical. For the 56 average 2DC size distributions, the average A_c/A_s is 1.38.

Using the CCM2 radiative transfer algorithms for ice (Briegleb 1992), the importance of this correction factor can be illustrated. For a 1-km thick cloud at temperature −50°C with an IWP of 10 (100 and 1000) g m^{-2}, including the A_c/A_s correction term, changes the albedo from 0.122 (0.233 and 0.524) to 0.128 (0.291 and 0.588) for a solar zenith angle of 0°. The albedo change is most significant for the 100 g m^{-2} IWP because there are larger aspherical particles, but τ is not so large that further increases have minimal impact on albedo. Therefore, the correction factor is significant and should be included in the parameterization.

A straightforward application of this parameterization is not always appropriate as some radiative features cannot be predicted from equal area spheres. For instance, Liou and Takano (1994) show that hexagonal ice crystals exhibit numerous halo and arc features that cannot be obtained from equal-projected area counterparts. For longwave radiative properties, Chylek and Videen (1994) show that although equal surface area cylinders approximate well the properties of hexagonal columns they are not suitable as equivalent particles for hexagonal plates.

5. Parameterization validity and implications

a. Representation of observed spectra

Figures 5, 7, and 11 show that parameterized size distributions represent the observed size distributions reasonably well. In this subsection, the adequacy of the parameterization is further explored.

First, the representation of small ice crystals measured by the VIPS is investigated. On average, the total area calculated from the small crystal parameterization using measured $\mathrm{IWC}_{<100}$ is 1.17 times that obtained from the VIPS measurements, with a standard deviation of 0.28. There is no noticeable trend for how this fraction varies with measured area. The fractions of mass, area, and number in different size ranges were compared for the measured and parameterized size distributions. On average, only 6% of the mass, 3% of the area, and less than 1% of the number are contained in sizes larger than those that this part of the parameterization is designed to represent. When examining the fractions of these quantities above and below other thresholds between 0 and 100 μm, the comparisons were also very good.

Estimates of parameterized quantities for crystals with $D_m > 100$ μm, represented by lognormal distributions, are just as good. For $\mathrm{IWC}_{>100}$ greater than 10^{-4} g m^{-3}, the total cross-sectional area from the parameterized lognormal distribution is on average 1.03 times that measured by the 2DC, with a standard deviation of 0.16. Detailed comparisons (figures not shown) of the mass, number, and areas above and below certain thresholds were performed. For thresholds greater than 400 μm, the parameterization slightly underestimates the IWC and area of larger crystal sizes, but on the whole the parameterization matches the data very well.

Previous observations have suggested that there may be two peaks in number distribution functions of ice crystals measured in cirrus (e.g., Varley 1978). As a result, Welch et al. (1980) parameterized ice crystal number density as two modified gamma distributions. An examination of the parameterized number distribution functions for varying IWC and T showed that a secondary peak is visible around 200 μm for large IWCs. When plotting mass distribution function, two peaks, corresponding to the large and small ice crystals, are seen at diameters of approximately 50 and 200 μm for IWCs between 10^{-1} and 10^{-3} g m^{-3} (figure not shown); the larger and smaller modes dominate the mass distribution function for larger and smaller IWCs, respectively. The 200-μm D_m peak location would roughly correspond to a 300-μm peak location for maximum crystal length, which is consistent with the peaks that MH found in mass distributions observed during CEPEX case studies.

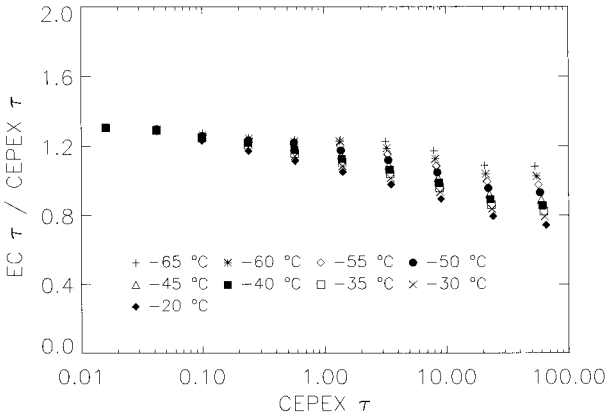

FIG. 13. Ratio of τ calculated using EC against τ calculated using current parameterization as function of τ calculated using this parameterization. The ratio A_c/A_s correction factor included. Different symbols represent different temperatures.

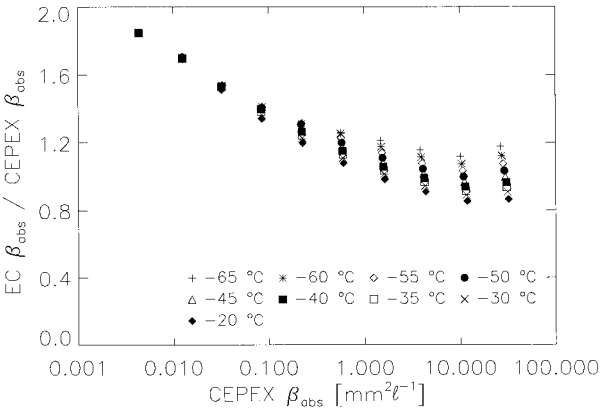

FIG. 14. As in Fig. 13 except for volume absorption coefficient β_{abs}.

b. *Comparisons with other radiative parameterizations*

In this subsection, optical properties obtained from this parameterization using ADT are compared with optical properties predicted from EC's parameterization. They parameterized ice cloud optical properties, such as optical thickness, single-scattering albedo, and emissivity, for use in climate models with IWP and r_e as independent variables. The current parameterization also allows calculations of *average* cloud optical properties but with temperature and IWC, instead of r_e and IWC, as independent variables.

To compare the two parameterizations for a given T and IWC, r_e must first be computed for the CEPEX parameterized size distributions. IWCs between 10^{-4} and $10^{-0.5}$ g m^{-3} and temperatures between $-65°$ and $-20°$C were used for comparing the parameterizations. All clouds were 1-km thick. These values are typical of those at which the measurements were made during CEPEX; the parameterizations should not be extrapolated outside these ranges, as the properties of ice crystals under such conditions might be different.

Using the CEPEX parameterization, the optical depth τ was calculated for a wavelength of 0.55 μm by integrating β_{ext} over the depth of the cloud. The spectral interval of 0.25 to 0.7 μm was used to calculate τ according to EC. Figure 13 shows the ratio of τ between the different parameterizations as a function of τ from CEPEX. The ratio of the EC τ to the CEPEX τ decreases as the temperature increases because the A_c/A_s term is larger for increasing temperatures. For larger τ, the most radiatively significant cases, there is a spread of $\pm 20\%$ because of the temperature dependence.

In Fig. 14, β_{abs}, calculated from the different parameterizations, are compared. A wavelength of 10 μm is used. The A_c/A_s correction term is needed to determine the projected area that is required for the calculation of β_{abs}. The agreement between the parameterizations is best for the more radiatively significant cases of larger absorption. The use of ADT to calculate Q_{abs} in the context of the CEPEX parameterization is somewhat of an approximation because it is based on the volumes of equivalent melted spheres; for more detailed applications in numerical models, these properties could be corrected by using a specific shape (e.g., hexagonal columns) and the mass-diameter relationships for that shape (e.g., Heymsfield et al. 1990).

Figure 15 shows a comparison of the single-scatter albedo calculated using the two different parameterizations in the spectral range 1.9–2.5 μm. The properly weighted β_{abs} and β_{ext}, computed at 12 different spectra intervals in this range, are used to determine $\tilde{\omega}_0$. The CEPEX $\tilde{\omega}_0$ are typically larger than those in the EC parameterizations, probably because there are proportionally more small crystals. However, when interpreting these differences it should be remembered that the data that EC used came from 2D probes, which have higher detection thresholds than the VIPS probe. These differences might become more significant when the

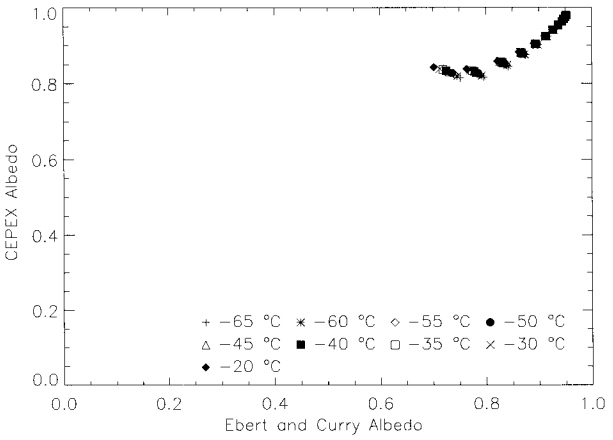

FIG. 15. Single scatter albedo calculated from EC against that calculated from CEPEX parameterization. Different symbols represent different temperatures.

TABLE 3. Ice water path, τ, albedo, emissivity (ϵ) calculated from different size distributions using two-stream radiative transfer code of CCM2. Also shown: r_e and percentage of mass from crystals with dimensions smaller than 20 μm. Here DR represents Dowling and Radke (1990). The numbers in brackets give IWP, τ, albedo, ϵ, and r_e when crystals smaller than 20 μm dimension are not considered in the calculations.

INPUT	IWP gm^{-2}	τ	Albedo	ϵ	$\%M < 20$ μm	r_e μm
CEPEX	1.02 (0.78)	0.17 (0.09)	0.10 (0.10)	0.10 (0.06)	23.5	16.2 (22.2)
	10.2 (9.5)	0.95 (0.74)	0.13 (0.12)	0.49 (0.43)	6.9	29.9 (35.7)
	40.9 (39.8)	2.7 (2.4)	0.19 (0.18)	0.87 (0.85)	2.7	43.5 (47.8)
	102.2 (101.0)	5.5 (5.1)	0.27 (0.26)	0.99 (0.98)	1.2	55.9 (58.9)
	204.3 (203.2)	9.2 (8.9)	0.36 (0.35)	1.00 (1.00)	0.5	67.6 (69.5)
	1022 (1021)	31.2 (31.1)	0.55 (0.55)	1.00 (1.00)	0.1	105.5 (105.8)
KKW	10.1 (9.5)	0.74 (0.48)	0.12 (0.11)	0.39 (0.32)	5.9	39.5 (57.7)
	101 (95)	7.4 (4.8)	0.35 (0.25)	0.99 (0.98)	5.9	39.5 (57.7)
	1012 (952)	73.5 (48.3)	0.71 (0.64)	1.00 (1.00)	5.9	39.5 (57.7)
DR	10.1 (10.1)	0.35 (0.34)	0.11 (0.11)	0.24 (0.24)	0.1	91.3 (91.8)
	101 (101)	3.5 (3.4)	0.20 (0.20)	0.94 (0.94)	0.1	91.3 (91.8)
	1013 (1012)	34.6 (34.4)	0.57 (0.57)	1.00 (1.00)	0.1	91.3 (91.8)
HP	0.32 (0.22)	0.05 (0.02)	0.10 (0.10)	0.03 (0.02)	16.0	18.9 (33.5)

multiple scattering events that can occur in a cloud are considered. Thus, even though there are not immense differences between the different parameterizations, they may be large enough to be detected in many physical situations. This issue is further discussed in the next section.

Reasonable agreement between the CEPEX parameterization and that of EC is not surprising because EC's parameterization assumes prior knowledge about the ice crystal size distribution, namely the value of r_e. The CEPEX parameterization has the added advantage that no advance knowledge about the shape of the size distribution, through r_e, is required. It should also be reiterated that the CEPEX parameterization can only be applied in tropical areas.

c. The role of small crystals

The importance of small ice crystals for causing high reflectances of tropical cirrus is currently being debated. Heymsfield and Miloshevich (1991) suggested that high cloud albedos might result from the presence of numerous ice crystals with dimensions smaller than 25 μm because the ratio of scattering to absorption efficiency increases as size decreases. Using a multiband, multistream radiative model with Mie theory, Stephens et al. (1990) also showed that for a fixed ice water path, distributions with smaller particles produced increasingly higher albedos.

Some observational studies have suggested that small crystals significantly affect the properties of cirrus. Knollenberg et al. (1993), hereafter KKW, measured ice crystals with dimensions from 0.1 μm to above 1 mm in the tops of cirrus during the Stratospheric–Tropospheric Exchange Project (STEP) and found particle mass modes at sizes of 20–40 μm; particles larger than 100 μm were rarely observed and IWCs were as high as 0.07 g m^{-3}. Other studies have not attributed the same importance to small ice crystals. Heymsfield and McFarquhar (1996) determined that the predominantly large particles in the lower, warmer parts of the cirrus contain at least an order of magnitude greater mass than those crystals in the colder tops and are equally important in producing high albedos.

Zender and Kiehl (1994) used a cloud model and the radiative transfer code of CCM2 to investigate the radiative sensitivities of tropical anvils to small ice crystals, which they defined to have dimensions between 3 and 20 μm. Using the observations of KKW as an initial condition, they showed that even though the small crystals accounted for less than 2% of the total cloud mass, the shortwave forcing and albedo were very sensitive to the presence of small crystals.

Their analysis is repeated here using several different input size distributions to investigate the sensitivities of the mass and radiative properties of cirrus to small ice crystals. A solar zenith angle of 0° is used for all calculations presented; similar trends were noted for calculations performed using solar zenith angles of 30° and 60°. The albedo, longwave emissivity, and optical depth were calculated for a column using the radiative transfer code of CCM2 with and without ice crystals between 3 and 20 μm. The distributions used are 1) the current CEPEX parameterization; 2) the parameterized form of KKW's observations used by Zender and Kiehl (1994); 3) HP's parameterized distribution; 4) Dowling and Radke's (1990) parameterized distribution; and 5) monodisperse size distributions with varying r_e.

Consistent with Zender and Kiehl (1994) and observations over the equatorial Pacific, all calculations assume a clear-sky albedo of 0.1. A 2-km thick cloud was assumed. The radiative transfer code is largely insensitive to cloud thickness, cloud base, and cloud top height, except when the specified parameterization depends on temperature. Table 3 shows albedos calculated using the first four distributions. The fractional contribution to the total mass by smaller crystals is also shown in Table 3. For the CEPEX distribution, mass is easily calculated from the distribution of equivalent melted spheres; for the other distributions, mass is calculated

using the mass diameter relationship of Brown and Francis (1995). This method replicates the more detailed calculations that account for size and shape (MH) within a factor of 2 or 3.

The contributions of small ice crystals to the mass and radiative properties can vary substantially. For an IWP of 100 g m^{-2} with the KKW distribution, the albedo decreases from 0.34 to 0.25 and τ from 7.4 to 4.8 when small crystals are not included. However, for the CEPEX parameterization under similar conditions, the albedo only decreases from 0.27 to 0.26 (τ from 5.5 to 5.1). From CEPEX, smaller crystals are fractionally more important for determining microphysical properties, especially mass, at low IWPs, but only cases with large IWPs are radiatively significant (i.e., produce high albedos), and for these cases small crystals do not dominate. For the Dowling and Radke (1990) input distribution small crystals are even less important, but small crystals contribute substantially (16 %) to the total mass of the HP distribution. However, their parameterization covers only measurements made under conditions of low IWCs and they did not measure crystals smaller than 20 μm; hence, any extrapolation of this distribution to larger IWCs or smaller crystals is not valid.

The measurements of KKW were made at very low temperatures of around -90°C, whereas the other measurements were made at temperatures higher than -65°C. This may explain some of the discrepancies in the roles of small crystals calculated using the different datasets. Different measurement techniques and the sampling of different cloud systems may also be partly responsible for explaining some of the differences.

6. Summary and conclusions

A parameterization that characterizes the average properties of tropical ice crystal size distributions, dependent on temperature and ice water content, IWC, has been developed. This parameterization is only valid for the average properties of blow-off anvils in the Tropics with total ice water contents between 10^{-4} and 1 g m^{-3} occurring at temperatures between $-70°$ and -20°C. It should not be used for clouds that occur for other conditions, especially those at mid and polar latitudes. It has great potential for use in climate and cloud-resolving models because it is mass conserving, provides easily integrable expressions for optical properties, and accurately represents the observed size distributions with mass equivalent diameters, D_m, smaller than 100 μm. The number distribution function is expressed as the sum of a first-order gamma distribution describing ''small'' ice crystals ($D_m < 100$ μm) and a lognormal distribution describing ''larger'' ice crystals ($D_m > 100$ μm). The two functions are added together to ensure easy integrability; each function does not contain significant numbers of crystals outside the size ranges it was designed to represent. The coefficients of the fit were chosen by least-squares fitting that forced the parameterized properties to replicate the observed properties as closely as possible. Even though the size distributions are represented in terms of melted equivalent diameters to force mass conservation, the calculated radiative properties are not those of equivalent melted spheres or equivalent area spheres. Uncertainty estimates were included so that future studies can examine the importance of size distribution variability. This error analysis showed that even though the determined relationships represent significant dependences in the data they do not account for all of the variability. There may not be a consistent relationship that explains all the variance observed, but this parameterization is still useful in that it reduces the unexplained variability. The following conclusions may also be noted.

1) The parameterized size distributions accurately represent the observed size distributions over the complete range of crystal sizes measured. The cross-sectional area and mass can easily be derived from the parameterization.
2) The shapes of the tropical size distributions substantially differ from those of midlatitude size distributions, especially at temperatures lower than -40°C.
3) Crystals with dimensions smaller than 20 μm do not contribute substantially to the optical properties of cirrus as calculated using the radiative transfer code of CCM2. This contradicts conclusions reached in some previous studies.
4) The optical properties calculated from this parameterization compare favorably with those predicted by Ebert and Curry (1992). Not as much (i.e., the effective radius) has to be known in order to apply the CEPEX parameterization.
5) Two separate modes in number and mass distribution function, centered at melted equivalent diameters of 50 and 200 μm, may exist depending on the temperature and IWC.

Acknowledgments. This research was supported in part by the Center for Clouds, Chemistry and Climate/Scripps Institution of Oceanography (C^4), and by the NSF Climate Dynamics Program, NSF Award No. ATM-9640613. The authors are grateful to Ramesh Srivastava and Al Cooper for their suggestions on the parameterization. We are appreciative of the contributions by Steve Aulenbach, who analyzed the VIPS data, and Walter Grotewold, who build the VIPS instrument. Donna Spikes helped with some of the preliminary parameterization calculations. The crew of the Learjet, especially Ray Hobbs, Dan Rusk, Rob Wallin, and Bruce Jones worked very hard to provide us with this dataset. Jeff Kiehl and Charlie Zender supplied the radiative transfer code that was used for some of the calculations. The authors are grateful to Jim Spinhirne and Bill Hart who generously supplied the lidar data that were used in the creation of Fig. 3. The comments of Bill Hall,

Wojciech Grabowski, Ilia Mazin, and three anonymous reviewers were greatly appreciated.

APPENDIX

Fit Parameter Determination

In order to calculate the best fit parameters of the gamma or lognormal functions, describing the observed size distributions, the chi-squared function, given by

$$\chi^2 = \sum_{i=1}^{N} \left(\frac{N_i - N(D_{m_i}; a_1, \cdots, a_M)}{\sigma_i} \right)^2, \quad \text{(A1)}$$

must be minimized. Here, N_i represents the observed number distribution function at mass-equivalent diameter D_{m_i}, and a_1 through a_M represent the fit parameters of the gamma ($M = 1$; $a_1 = \alpha_{<100}$) or lognormal distribution ($M = 2$; $a_1 = \mu_{>100}$; $a_2 = \sigma_{>100}$). The σ_i represent the uncertainties associated with the data points.

The measurement uncertainties arise from statistical fluctuations in the number of measurements [i.e., a Poisson distribution with variance given by the function $N(D_m; a_1, \ldots, a_M)$] and the uncertainty associated with the measurement of an individual particle (nonexistent for number, area of an individual particle when minimizing for area distributions). Here, the statistical error is always dominant. Hence, the σ_i are given by expressions such as

$$\sigma_i = \frac{M_i^{1/2}}{V_i}, \quad \text{(A2)}$$

where $M_i = N(D_{m_i}; a_1, \cdots, a_M)\ V_i$ is the number of ice crystals that would have been counted in the ith bin if the modeled distribution function is correct, and V_i is the sample volume for the appropriate size bin. To minimize the difference between observed and parameterized area (which is closely related to the radiative properties because parameters such as the volume extinction coefficient are proportional to the projected area of the measured particles), Eq. (A1) is still valid because the uncertainties σ_i in the denominator, as well as the numerator in Eq. (A1), both increase by an amount proportional to the observed area and hence cancel.

The downhill simplex method (Presset al. 1992, 402) is used to determine the fit parameters minimizing χ^2. The bootstrap method (Efron and Tibshirani 1993), a modified Monte Carlo technique, gives uncertainty estimates on the parameters that are needed to give some measure of how much the ice crystal size distributions can vary. Fitting methods that use the derivatives of the fit functions, such as the Levenberg–Marquardt method, assume that the measurement errors are normally distributed (see Press et al. 1992, p 686) and are not applicable as it is not known whether the measurement errors were normally distributed. The use of the statistically robust bootstrap method is appropriate when not enough is known about the underlying process or the nature of the measurement errors.

To use the bootstrap, the dataset, assumed to consist of M independent and identically distributed data points, is used to generate a synthetic dataset, also with M data points, by randomly drawing M data points *with replacement* from the original dataset. Specifically, for the large crystal distributions, assume that M separate size distributions were used to calculate the average size distribution for a given IWC and T bin. Then, M size distributions are randomly drawn from this sample to create a new averaged size distribution for which the fit parameters are reestimated. This process is repeated a number of times, the standard deviation of each fit parameter providing a measure of its variation. For the gamma distribution characterizing the small ice crystal size distributions measured by the VIPS, M particles are drawn at random from the M measured particles. This generates a new size distribution to be used in the computations; averages and standard deviations of the fit parameters can then be obtained as above. Hence, the needed confidence limits on the estimated model parameters may be established.

REFERENCES

Arnott, W. P., Y. Dong, J. Hallett, and M. R. Poellot, 1994: Role of small ice crystals in radiative properties of cirrus: A case study, FIRE II, 22 November 1991. *J. Geophys. Res.,* **99,** 1371–1381.

Borovikov, A. M., L. I. Gaivoronskii, E. G. Zak, V. V. Kostarev, I. Z. Mazin, V. E. Minervin, A. Kh. Khrgian, and S. M. Shmeter, 1963: *Cloud Physics.* Israel Program for Scientific Translations, 392 pp.

Briegleb, B. P., 1992: Delta–Eddington approximation for solar radiation in the NCAR community climate model. *J. Geophys. Res.,* **97,** 7603–7612.

Brown, P. R. A., and P. N. Francis, 1995: Improved measurements of the ice water content in cirrus using a total-water probe. *J. Atmos. Oceanic Technol.,* **12,** 410–414.

Chylek, P., and G. Videen, 1994: Longwave radiative properties of polydispersed hexagonal ice crystals. *J. Atmos. Sci.,* **51,** 175–190.

Committee on Earth Sciences, 1989: Our changing planet: The FY 1990 U.S. Global Change Research Program, U.S. Geological Survey, 118 pp. [Available from U.S. Global Change Research Program, 12201 Sunrise Valley Drive, Reston, Va., 22092.]

Dowling, D. R., and L. F. Radke, 1990: A summary of the physical properties of cirrus clouds. *J. Appl. Meteor.,* **29,** 970–978.

Ebert, E. E., and J. A. Curry, 1992: A parameterization of ice cloud optical properties for climate models. *J. Geophys. Res.,* **97,** 3831–3836.

Efron, B., and R. J. Tibshirani, 1993: *An Introduction to the Bootstrap.* Chapman and Hall, 436 pp.

Feingold, G., and Z. Levin, 1986: The lognormal fit to raindrop spectra from frontal convective clouds in Israel. *J. Climate Appl. Meteor.,* **25,** 1346–1363.

Griffith, K. T., S. K. Cox, and R. G. Knollenberg, 1980: Infrared radiative properties of tropical cirrus clouds inferred from aircraft measurements. *J. Atmos. Sci.,* **37,** 1077–1087.

Heymsfield, A. J., 1977: Precipitation development in stratiform ice clouds: A microphysical and dynamical study. *J. Atmos. Sci.,* **34,** 367–381.

——, 1986: Ice particles observed in a cirriform cloud at −83°C and implications for polar stratospheric clouds. *J. Atmos. Sci.,* **43,** 851–855.

——, and C. M. R. Platt, 1984: A parameterization of the particle

size spectrum of ice clouds in terms of ambient temperature and the ice water content. *J. Atmos. Sci.,* **41,** 846–855.

——, and L. M. Miloshevich, 1991: Limit to greenhouse warming? *Nature,* **351,** 14–15.

——, and G. M. McFarquhar, 1996: On the high albedos of anvil cirrus in the tropical Pacific warm pool: Microphysical interpretations from CEPEX. *J. Atmos. Sci.,* **53,** 2424–2451.

——, K. M. Miller, and J. D. Spinhirne, 1990: The 27–28 October 1986 FIRE IFO cirrus case study: Cloud microstructure. *Mon. Wea. Rev.,* **118,** 2313–2328.

Hobbs, R., B. Morrison, R. Ashenden, and R. F. Ide, 1996: Comparison of two data processing techniques for optical array probes. *FAA Int. Conf. on Aircraft Inflight Icing,* Springfield, VA, FAA, 69–90.

Kinne, S., T. P. Ackerman, A. J. Heymsfield, F. P. J. Valero, K. Sassen, and J. D. Spinhirne, 1992: Cirrus microphysics and radiative transfer: Cloud field study on 28 October 1986. *Mon. Wea. Rev.,* **120,** 661–684.

Knollenberg, R. G., A. J. Dascher, and D. Huffman, 1982: Measurements of the aerosol and ice crystal populations in tropical stratospheric cumulonimbus anvils. *Geophys. Res. Lett.,* **9,** 613–616.

——, K. Kelly, and J. C. Wilson, 1993: Measurements of high number densities of ice crystals in the tops of tropical cumulonimbus. *J. Geophys. Res.,* **98,** 8639–8664.

Kosarev, A. L., and I. P. Mazin, 1989: Empirical model of physical structure of the upper level clouds of the middle latitudes. *Radiation Properties of Cirrus Clouds,* Nauka, 29–52.

Liou, K. N., and Y. Takano, 1994: Light scattering by nonspherical particles: Remote sensing and climatic implications. *Atmos. Res.,* **31,** 271–298.

McFarquhar, G. M., and A. J. Heymsfield, 1996: Microphysical characteristics of three cirrus anvils sampled during the Central Equatorial Pacific Experiment. *J. Atmos. Sci.,* **53,** 2401–2423.

Mitchell, D. L., and W. P. Arnott, 1994: A model predicting the evolution of ice particle size spectra and radiative properties of cirrus clouds. Part II: Dependence of absorption and extinction on ice crystal morphology. *J. Atmos. Sci.,* **51,** 817–832.

Platt, C. M. R., and Harshvardhan, 1988: Temperature dependence of cirrus extinction: Implications for climate feedback. *J. Geophys. Res.,* **93,** 11 051–11 058.

Press, W. H., S. A. Teukolsky, W. T. Vetterling, and B. P. Flannery, 1992: *Numerical Recipes in FORTRAN. The Art of Scientific Computing,* 2nd ed. Cambridge University Press, 963 pp.

Ramaswamy, V., and V. Ramanathan, 1989: Solar absorption by cirrus clouds and the maintenance of the tropical upper troposphere thermal structure. *J. Atmos. Sci.,* **46,** 2293–2310.

Roeckner, E., U. Schlese, J. Biercamp, and P. Loewe, 1987: Cloud optical depth feedback and climate modeling. *Nature,* **329,** 138–140.

Spinhirne, J. D., and W. D. Hart, 1990: Cirrus structure and radiative parameters from airborne lidar and spectral radiometer observations: The 28 October 1986 FIRE study. *Mon. Wea. Rev.,* **118,** 2329–2343.

Stephens, G. L., S. Tsay, P. W. Stackhouse Jr., and P. J. Flatau, 1990: The relevance of the microphysical and radiative properties of cirrus clouds to climate and climate feedback. *J. Atmos. Sci.,* **47,** 1742–1753.

Sundqvist, H., 1978: A parameterization scheme for non-convective parameterization including prediction of cloud water content. *Quart. J. Roy. Meteor. Soc.,* **104,** 677–690.

Thekaekara, M. P., and A. J. Drummond, 1971: Standard values for the solar constant and its spectral components. *Nat. Phys. Sci.,* **229,** 6–9.

van de Hulst, V. C., 1956: *Light Scattering by Small Particles.* Dover Publications, 182 pp.

Varley, D. J., 1978: Cirrus particle distribution study, Part I. Air Force Geophysical Laboratory Rep. AFGL-TR-78-0192, 71 pp. [Available from Air Force Geophysical Laboratory, Hanscom Air Force Base, MA 01731.]

Warren, S. G., 1984: Optical constants of ice from the ultraviolet to the microwave. *Appl. Opt.,* **23,** 1206–1225.

Welch, R. M., S. K. Cox, and J. M. Davis, 1980: *Solar Radiation and Clouds. Meteor. Monogr.,* No. 39, Amer. Meteor. Soc., 93 pp.

Zender, C. S., and J. T. Kiehl, 1994: Radiative sensitivities of tropical anvils to small ice crystals. *J. Geophys. Res.,* **99,** 25 869–25 880.